Full Length Article

In-flow photocatalytic oxidation of NO on glasses coated with nanocolumnar porous TiO$_2$ thin films prepared by reactive sputtering

Ramón Azpiroz [a], Enrique Carretero [b,*], Ana Cueva [b], Aida González [a,c], Manuel Iglesias [a,*], Jesús J. Pérez-Torrente [a,*]

[a] Departamento de Química Inorgánica, Instituto de Síntesis Química y Catálisis Homogénea-ISQCH, Universidad de Zaragoza-C.S.I.C., 50009 Zaragoza, Spain
[b] Departamento de Física Aplicada, Universidad de Zaragoza, C/Pedro Cerbuna, 12, 50009 Zaragoza, Spain
[c] Ariño Duglass, Pol. Ind. Royales Bajos s/n, 50171 Puebla de Alfindén (la), Zaragoza, Spain

ABSTRACT

The magnetron sputtering technique has been successfully employed for the preparation of porous TiO$_2$ thin films on soda-lime glasses by means of an oblique angle deposition strategy. The morphology of the thin layers is affected by the deposition parameters, such as, the angle with respect to the target, applied power, total pressure, oxygen pressure and deposition time. It has been shown that 60–65° angles, lead to a compromise between the porosity, the level of oxidation and the thickness of the film. High total pressures of the deposition process result in less dense coatings of greater porosity. Moreover, the oxygen flow during the deposition process must be carefully adjusted for each set of deposition conditions, in order to achieve an optimum degree of oxidation. The evaluation of coated-glasses in the in-flow photocatalytic oxidation of nitrogen oxide has shown that the presence of a porous film is essential to achieve photocatalytic activity. The best performing coated-glass was able to reduce the NO concentration ca. 20% for 5 h. SEM and TEM images of this film show a microstructure composed of nanometric grains and a tilted columnar structure. Nanocrystal electron diffraction, XRD and Raman spectroscopy have confirmed the deposition of TiO$_2$ anatase.

1. Introduction

Air pollution in general, and photochemical smog in particular, have been reported to cause severe damage to the environment and human health [1]. In this regard, nitrogen oxides (NO$_x$) are decisive contributors to the buildup of photochemical smog in urban areas, which is deemed responsible for acidic depositions, as well as cardiovascular and respiratory disorders [2–4]. From this perspective, the design of NO$_x$-control methodologies and devices that can be straightforwardly integrated within the urban landscape is pivotal to enhance the living conditions of the inhabitants of metropolitan areas.

The reduction of NO$_x$ concentration via photocatalytic oxidation to furnish nitrates has shown great promise for the control of air pollution. Among the photocatalytic materials hitherto reported, titanium dioxide (TiO$_2$) has been one of the most successful and broadly studied [5–8]. The oxidation of NO$_x$'s on TiO$_2$ surfaces usually requires UV irradiation, owing to the fact that these materials typically present band-gaps that span from ca. 3.0 to 3.2 eV. However, it must be mentioned that some

TiO$_2$-doped materials have proved able to operate under visible light irradiation [9].

In the presence of oxygen and moisture, UV-irradiation of TiO$_2$ surfaces generates radical species, mainly OH● and O$_2^-$●, which prompt the oxidation of nitrogen oxides. These species are formed by the reaction of adsorbed H$_2$O or O$_2$ molecules with a charge carrier generated from an electron-hole pair (Fig. 1) [10].

The removal of nitrogen oxides by photocatalytic methods has been standardized by the ISO 22197-1:2007 [11], which employs nitric oxide (NO) as substrate (Scheme 1).

TiO$_2$ coatings on various types of construction materials, such as, ceramic tiles, asphalt or glass, show potential for the integration of photocatalytic materials in the urban environment [12–14]. The latter is of great interest due to the large glazed surfaces present in the façades of buildings and skyscrapers in major cities. However, for commercial applications, the coated-glasses must comply with a series of aesthetic and durability requirements; for example, transparency of the final hybrid material and robust adhesion of the film layer to the glass

substrate. These prerequisites limit the types of techniques that can be employed in the deposition of the TiO$_2$ coating. In this context, TiO$_2$ deposition by magnetron sputtering emerges as a promising method for the preparation of thin films with appropriate mechanical and visual properties. Moreover, sputtering techniques are already implemented in the glass industry for the manufacture of self-cleaning, solar-control or low-emissivity glazing.

Magnetron sputtering is a physical vacuum deposition (PVD) technique that consists on the evaporation of a solid material (target) by ion bombardment of a process gas, typically a noble gas such as Ar [15]. Additionally, a reactive gas can be added to react with the evaporated material to form a layer of a compound material. In particular, to form a TiO$_2$ thin film it is necessary to use a Ti target and O$_2$ as a reactive gas. Magnetron sputtering has the advantage that it is a scalable technique and that it allows great control over the thickness of the deposited layer. This technique allows depositing a material with different composition, morphologies and crystalline structures depending on various deposition parameters that require optimization [16,17].

The use of sputtering techniques allows the deposition of TiO$_2$ films in the anatase phase [18–20]. Anatase, rutile and brookite are the three crystallographic forms of TiO$_2$, and, although their activity and stability depend on the agglomeration, particle size and the type of support [21–25], anatase is often the most active polymorph [26–28]. The higher activity of anatase relative to rutile has been attributed to various factors, which include a greater surface area, more active sites, and improved redox capability (due to a slightly larger band-gap) in the case of the former. Moreover, the porosity of the material, either attained by the actual nature of the support or by the intrinsic porosity of the TiO$_2$ coating, plays a crucial role in the activity of the photocatalyst [29].

The deposition of materials by magnetron sputtering results in compact and high-density films. Therefore, to achieve porous materials it is necessary to use special settings and adjust the various deposition parameters. In this context, it is known that a porous material can be achieved by modifying the angle of inclination between the target and the substrate, this configuration is known as oblique angle deposition (OAD) [30–33]. On the other hand, the morphology of the thin layers is also affected by other deposition parameters such as the total pressure and deposition temperature [34,35]. High pressure and low temperature deposition can promote the formation of a columnar structure consisting of tapered units defined by voided growth boundaries.

The photocatalytic activity of TiO$_2$ films deposited by sputtering processes has been explored in the degradation of a variety of organic molecules; e.g., methylene blue [36–38], phenol [39], methanol [40], trichloroethylene and ethylene [41]. However, as opposed to TiO$_2$ materials deposited by other methods [42,43], the in-flow oxidation of NO (g) has not yet been reported for their sputtered counterparts as far as we are aware. We report herein on the preparation and characterization of glasses coated with a porous TiO$_2$-anatase thin film deposited by reactive sputtering and their application in the in-flow degradation of NO(g).

$$NO + 2HO^\bullet \longrightarrow NO_2 + H_2O$$

$$NO_2 + HO^\bullet \longrightarrow NO_3^- + H^+$$

$$NO + O_2^{-\bullet} \longrightarrow NO_3^-$$

Scheme 1. Set of equations that describe the photocatalytic oxidation of NO at TiO$_2$ surfaces.

2. Experimental

2.1. Preparation of porous TiO$_2$ thin films on glass for photocatalytic coatings

The photocatalytic studies were carried out on flat soda-lime glasses of 100 mm × 50 mm × 6 mm (height, width and thickness) manufactured by Guardian. The glasses were cleaned with a liquid detergent, rinsed with water and dried on absorbent paper. The glasses were then coated with a 10 nm thin film of SiO$_2$ and a thin film of TiO$_2$ deposited both by PVD (Physical Vapor Deposition). The thin films were deposited by magnetron sputtering in an in-line deposition system with a target size of 600 mm × 100 mm. The deposition of the SiO$_2$ film was carried out dynamically (sample moving with respect to the target) to guarantee a homogeneity in its thickness of approximately 10 nm. This film was deposited with a Si target (99.99 % purity) by means of reactive sputtering applying a power of 1500 W (2.5 W/cm^2) with an Argon flow of 160 sccm and 40 sccm of O$_2$, equivalent to a total pressure of 0.15 Pa. The deposition of the TiO$_2$ films was carried out statically at different angles (between 36° and 77°) with respect to the target. This film was deposited with a Ti target (99.99 % purity) by means of reactive sputtering applying different deposition conditions. After the deposition process, coated-glasses were subjected to thermal annealing in a Thermolyne furnace type 30400 using the following temperature program: starting at room temperature, heated at a rate of 7 °C/min up to 550 °C (75 min), held for 1 h at 550 °C and allowed to cool slowly over several hours.

2.2. Characterization of porous TiO$_2$ thin films on glass

Scanning Electron Microscopy (SEM) and High-Resolution Transmission Electron Microscopy (HRTEM) images were obtained using eSEM-FEI QuantaTM 250 and FEI Titan 80–300 TEM microscopes, respectively, at the Structural-Morphology Characterization Service of CIC NanoGUNE. A thin sample for TEM was prepared using dual-beam instrument FEI Helios 450 with standard lift out and thinning protocols [44]. Raman and UV–vis spectra were performed at the Chromatography and Spectroscopy Service of the ISQCH. Raman spectra were recorded on a JASCO NRS 3100 dispersive Raman spectrometer, equipped with a high-performance green laser (532 nm, 20 mW) and 1800 ln grating. The spectra are the result of subtracting the glass signal
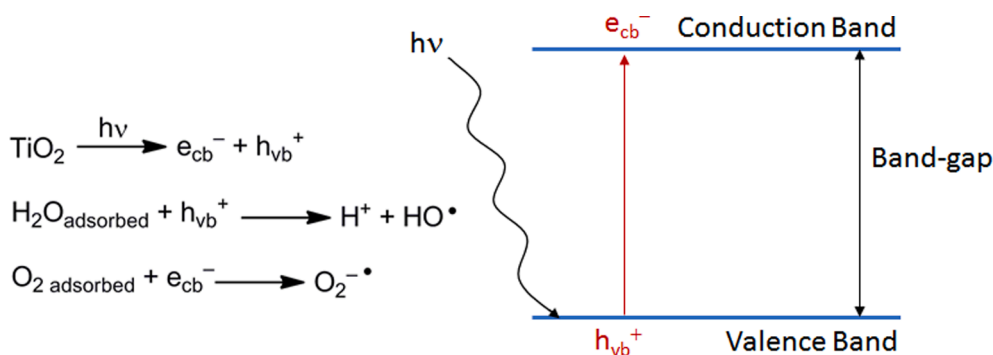

Fig. 1. Formation of O$_2^-\bullet$ and OH• radicals (left) and schematic representation of electron-hole generation (right).

to the Raman spectra obtained from the coated-glasses. UV–vis spectra were recorded on a Jasco V-670 dual beam spectrophotometer, using a clean uncovered glass as reference sample. Bandgaps were determined by Tauc plot method [45] using the bandgap calculation subroutine embedded in Jasco Spectra Analysis software. X-ray diffraction measurements were carried out at the X-ray Diffraction and Fluorescence Analysis Service of the Universidad de Zaragoza. XRD patterns were recorded on a RIGAKU diffractometer equipped with a rotating Cu anode, model Ru2500, operating at 40 Kv and 80 mA using a graphite monochromator to select the CuKα radiation. Data were collected in a 2θ range of 20–60°, step = 0.03°, t = 3 s/step. Thickness measurements were obtained with a Dektak XT mechanical profilometer whose typical error is approximately 1 nm. The X-ray photoelectron spectroscopy (XPS) analyses were carried out using a Kratos Axis Supra spectrometer at the Laboratory of Advanced Microscopy of the Institute of Nanoscience of Aragón. The photoelectron spectra were excited by a soft X-ray Al Kα (1486.6 eV) anode at a power of 120 W (8 mA, 15 kV). Spectra have been charge corrected to the main line of the C 1s spectrum (adventitious carbon) set to 284.8 eV. Peak fitting was performed with CasaXPS software, using weighted Gaussian/Lorentzian product functions after Shirley background subtraction.

2.3. Measurement of the photocatalytic activity of coated-glasses in NO (g) oxidation

The photocatalytic activity of the coated-glasses was measured in an inert flat-bed photoreactor designed and manufactured by the company Ariño Duglass according to ISO 22197-1:2007 [11]. The experimental setup comprises a gas supply system, a photoreactor, and an analysis system (Fig. 2). The photoreactor consists of a stainless-steel reaction compartment, suitable to hold 50 cm^2 glass samples (50 mm × 100 mm) of variable thicknesses on Teflon holders, equipped with a borosilicate glass window. The irradiation source was a 36 W black light (Philips Actinic BL TL-DK, 340–400 nm with a maximum at 370 nm) placed over the reactor at 6.5 cm from the sample with an irradiance (incident power/area) of 10 W/m^2. The reactor is fed with a NO/N$_2$ certified mixture as polluting gas (120 ppm of NO) and high purity synthetic air. Humidity control was achieved by bubbling an air stream through a gas wash bottle containing water. The dry air, moist air and N$_2$/NO streams were regulated with mass flow controllers (Bronkhorst, F-201CV) and mixed to obtain the desired NO(g) concentration. The system is equipped with a stainless-steel static gas mixer (Koflo Pipe Mixer) upstream of the reactor inlet, and temperature and humidity sensors at the reactor inlet and outlet. The gas flows were: 1.50 and 1.47 L/min for dry and wet synthetic air, respectively, and 30 mL/min for the N$_2$/NO polluting gas. After a stabilization period for purging the experimental system with the gas mixture, typically 1 h, the concentration of NO(g) through the reactor was 1 ± 0.05 ppm with a flow rate of 3 L/min. NO(g) and NO$_2$(g) concentrations in the outlet gas stream from the photoreactor were continuously monitored by using electrochemical gas sensors (Alphasense Ltd, NO-A4 and NO$_2$-A4F3). The concentration of both gases, temperature and humidity data were recorded in a computer using software designed by the Electronic Instrumentation Service from the University of Zaragoza. The outlet gas stream was bubbled trough a concentrated NaOH solution in a gas wash bottle.

The photocatalytic experiments were performed at room temperature with a relative humidity of 50 % at 25 °C. The measurements were carried out continuously for 4–6 h with data collection every 7 s. At the end of the measurement, the coated-glasses were washed with distilled water in order to determinate the NO$_2^-$ and NO$_3^-$ concentration using a colorimetric indicator from Hasch. Coated-glasses with significant photocatalytic activity were washed with Milli-Q water, dried on an absorbent paper and subjected to successive photocatalytic cycles every 24 h under the same conditions.

3. Results and discussion

3.1. Porous TiO$_2$ thin films on glass as precursors for photocatalytic coatings for NO(g) oxidation

3.1.1. Parameters for the deposition of porous TiO$_2$ thin films

Porous TiO$_2$ thin films were deposited on flat soda-lime glasses coated with a 10 nm thin film of SiO$_2$ by reactive magnetron sputtering. The role of the SiO$_2$ coating is to inhibit the diffusion of alkaline ions from the glass substrate to the photocatalytic coating during the annealing process [46,47] and to provide thermal stability to the TiO$_2$ coating through the formation of covalent Ti-O-Si bonds [12b]. Since oblique angle deposition (OAD) is required to obtain porous TiO$_2$-anatase films, one of the parameters studied in this work is the deposition by varying this angle. A schematic representation of the deposition system is shown in Fig. 3, where α is the zenith angle of the center of the sample with the center of the target. To deposit at this fixed angle, the carrier must be in a static position. The distance d is a fixed value, 10 cm, of the in-line deposition system used.

The deposition angle strongly influences the film properties, the main one being the porosity. In addition, the greater the α angle, the lower the deposition rate will be, since the sample will be further away and subtends a smaller solid angle seen from the target. The deposition
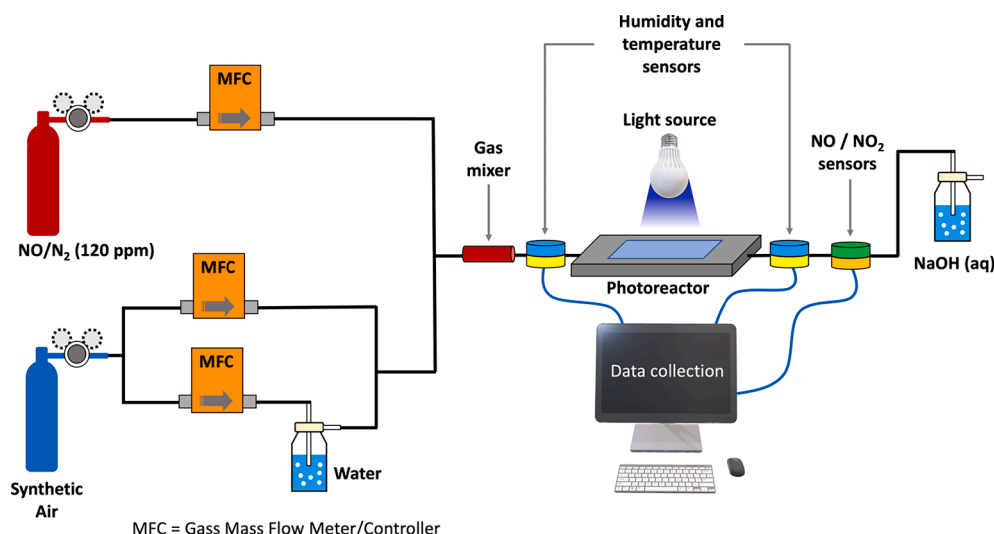

Fig. 2. Schematic representation of the experimental setup for the in-flow photocatalytic oxidation of NO(g).
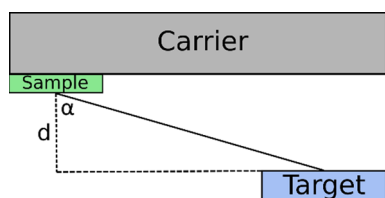
Fig. 3. Descriptive diagram of the sample position relative to the target in the deposition chamber.

angle also affects the thickness of the sample, which results in a great inhomogeneity throughout the length of the film. An example of this inhomogeneity is presented in Table 1, which shows the change in thickness of a sample measured at points with different α angle.

The thickness of the film—which can be tuned by changing the deposition time—plays a crucial role in the photocatalytic activity of the sample, with lower thicknesses leading to reduced catalytic performances (*vide infra*). Another key aspect which is affected by the deposition angle is the degree of oxidation of the film. It has been observed that low α angles lead to formation of sub-oxidized films, which are characterized by black-opaque areas; while, in the case of high α angles, the titanium coating is completely oxidized and a dielectric and transparent film is obtained. The degree of oxidation can be adjusted by modifying the oxygen flow during the deposition process. The highest photocatalytic activities were observed for samples in the transition zone, that is, between totally oxidized and sub-oxidized films, since, although the "as deposited" samples are partially sub-oxidized, they will complete the oxidation process during the thermal treatment at high temperature (see Figs. S1 and S2 in the Supplementary Material).

In order to optimize the deposition parameters, and to maximize the photocatalytic activity, a set of coated-glasses were prepared to study the influence of: i) the deposition angle, ii) the Ar flow, iii) the applied power, and iv) the deposition time. The identification of the samples, as well as the parameters used in their fabrication, are shown in Table 2.

3.1.2. Influence of the deposition angle

Initially we fabricated four coated-glasses **G1** – **G4** with deposition angles (α) of 77, 72, 63 and 36°, respectively, under the following standard deposition conditions: Ar flow 600 sccm, O_2 flow 40 sccm, applied power of 5000 W and a deposition time of 40 min (Table 2). The photocatalytic activity in the degradation of NO(g) of the coated-glasses is shown in Fig. 4a.

Except for the sample **G1**, which was prepared with a higher deposition angle, the coated-glasses exhibited photocatalytic activity. In particular, the photocatalytic activity of the glass **G3**, prepared with a deposition angle of 63°, is remarkable. Once the irradiation source is turned on, a peak of activity is observed with a reduction of NO(g) concentration of 0.87 ppm and NO_2(g) formation of 0.23 ppm. The NO(g) concentration remains practically constant at 0.80 ppm, and that of the generated NO_2(g) at 0.14 ppm, from the second hour of the experiment until the irradiation source is turned off. The initial sharp decrease in NO(g) concentration is attributed to NO(g) chemisorption in the porous network of the coating which is diagnostic of the porosity of the coating. The photocatalytic activity of glasses **G2** and **G4** is comparable with NO(g) stabilization values of 0.87 and 0.91 ppm, respectively.

Table 1
Coating thickness as a function of deposition angle.

α (°)	thickness (nm)
62.6	820
64.3	712
65.9	480
66.8	406

Table 2
TiO_2-anatase coated-glasses prepared by reactive magnetron sputtering and the deposition conditions used in their fabrication. All samples were deposited at an O_2 flow rate of 40 sccm.[a]

Sample	α(°)	Ar flow (sccm)	Power (W)	Deposition time (min)
G1	77	600	5000	40
G2	72			
G3	63			
G4	36			
G3.1	63	160	5000	40
G3.2		600		
G3.3		1000		
G3.4		2000		
G3.2a	63	600	3000	60
G3.2b			4000	50
G3.2c			5000	40
G3.2c_5	63	600	5000	5
G3.2c_10				10
G3.2c_20				20
G3.2c_40				40

[a] Note that G3, G3.2, G3.2c and G3.2c_40 are the same sample.

3.1.3. Influence of the argon flow

In order to investigate the effect of the total pressure on the photocatalytic activity of the resulting coatings, we have fabricated three new coated-glasses with a deposition angle of 63° under the standard deposition conditions at different argon flows: 160, 600, 1000 and 2000 sccm, which have been labelled as **G3.1** – **G3.4**, respectively. The photocatalytic activity in the degradation of NO(g) of these coated-glasses is shown in Fig. 4b. Glass **G3.3**, fabricated with an Ar flow of 1000 sccm, slightly outperforms the photocatalytic activity of **G3.2**, since the NO(g) values were below 0.80 ppm throughout the experiment (0.71–0.74 ppm), with NO_2(g) formation values close to 0.13 ppm. The photocatalytic behavior of glass **G3.4**, fabricated with an Ar flow of 2000 sccm, was however similar to that of **G3.2** with a NO(g) stabilization value close to 0.80 ppm. These results show that the increase of the total pressure has a positive influence on photocatalytic activity. Conversely, a decrease in the Ar flow to 160 sccm suppresses the photocatalytic activity as observed for sample **G3.1**. These results agree with the microstructure of sputter-deposited coatings reported by Thornton [15b], where low total deposition pressure results in a denser and more compact coating with lower porosity.

G3 and **G4** were also deposited at an O_2 flow rate of 60 sccm. A comparison of the photocatalytic activity of these coated-glasses with those fabricated at a flow rate of 40 sccm is shown in Fig. 5. The photocatalytic performance of glass **G3** (60 sccm O_2) is worse than that of glass **G3** (40 sccm O_2). However, glass **G4** (60 sccm O_2) slightly outperforms the photocatalytic activity of **G4** (40 sccm O_2), with an initial decrease of the NO(g) concentration to 0.30 ppm and a stabilization value of 0.89 ppm. These results highlight the positive effect of increasing the O_2 flow rate when the deposition is carried out at low deposition angles in order to obtain less sub-oxidized coatings.

3.1.4. Influence of the applied power

With the aim of studying the effect of the applied power on the photocatalytic performance, we have prepared two new coated-glasses with the optimized deposition angle (63°) under the standard deposition conditions with applied powers of 3000, 4000 and 5000 W, which have been labelled as **G3.2a** – **G3.2c**, respectively. As can be seen in Fig. 4c, decreasing the applied power to 4000 and 3000 W has a negative impact on the photocatalytic activity despite increasing the deposition time to 50 and 60 min, respectively. The deposition time was increased with decreasing power to compensate for the lower deposition rate. Although the coated-glass **G3.2b** performs well at the beginning of the experiment, its activity decreases after the second hour to be below that of the glass **G3.2c**, prepared with 5000 W, with NO(g) concentration of 0.83 ppm.
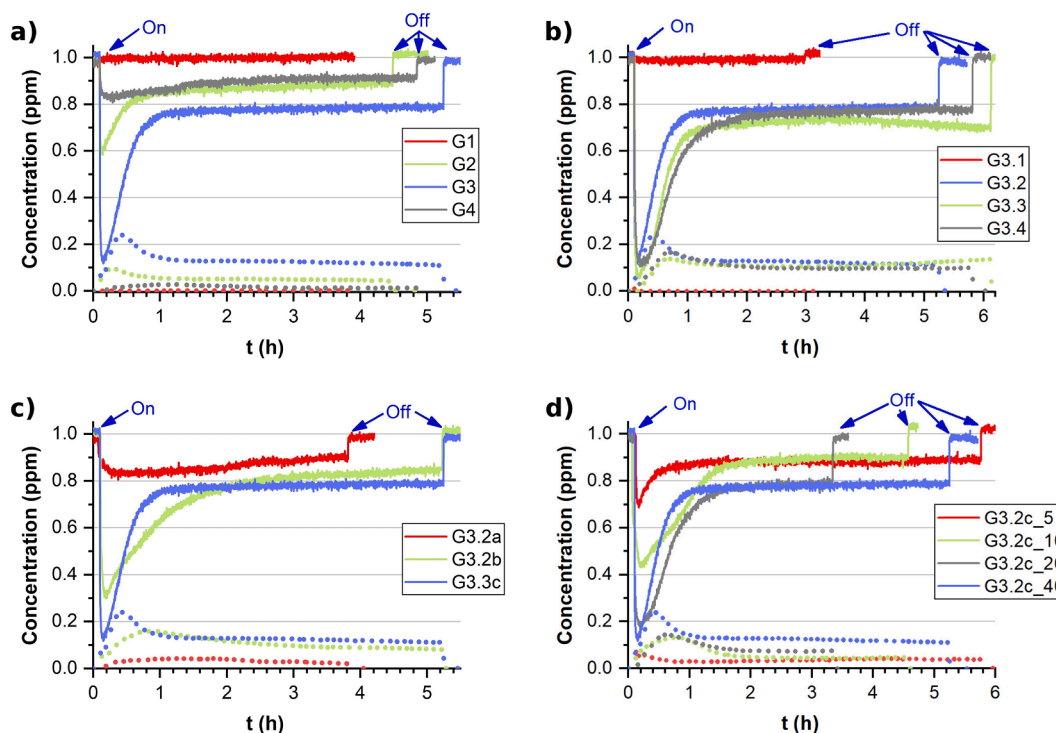
Fig. 4. Photocatalytic activity in the degradation of NO(g) (solid line) and formation of NO$_2$(g) (dot line) of coated-glasses under different deposition conditions: a) deposition angle, b) argon flow, c) applied power and d) deposition time (see Table 2).
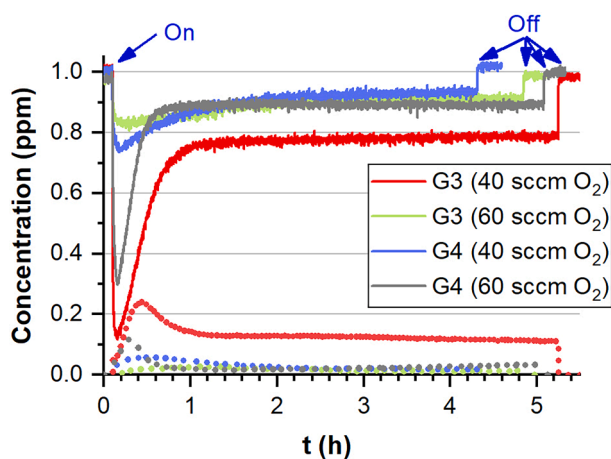

Fig. 5. Photocatalytic activity in the degradation of NO(g) (solid line) and formation of NO$_2$(g) (dotted line) of coated-glasses **G3** and **G4** at O$_2$ flow rates of 40 and 60 sccm.

It is worth noting that reducing the deposition power decreases the deposition rate, which may lead to fully oxidized thin films. In addition, when this parameter is modified, the optimum oxygen flow rate may change, making it difficult to optimize both parameters. Thus, we consider 5000 W and 40 sccm of O$_2$ to be the most suitable conditions because thin films with good photocatalytic activity and high rate of deposition are achieved.

3.1.5. Influence of the deposition time

In view of the good catalytic performance exhibited by the coated-glass **G3.2c** (deposition time of 40 min), we decided to study the effect of decreasing the deposition time to 5, 10 and 20 min under the same conditions (see Table 2). The photocatalytic activity of the coated-glasses, labelled as **G3.2c_5** – **G3.2c_20**, was compared with that of

G3.2c_40, prepared with a deposition time of 40 min (Fig. 4d). The thickness of the deposited TiO$_2$ thin film is approximately proportional to the deposition time. Thus, as expected, a reduction in photocatalytic activity was observed with decreasing deposition time, which is associated with a decrease in film thickness. However, it was observed that the photocatalytic performance of the coated-glass **G3.2c_20**, prepared with half the deposition time, is similar to that of **G3.2c_40**. This indicates that above a minimum thickness the photocatalytic activity does not improve.

According to Table 1, the thickness of TiO$_2$ in the center of sample **G3.2c_40** is approximately 800 nm. This suggests that as **G3.2c_20** has been deposited for half the time, its thickness should be half, so that increasing the thickness by 400 nm only marginally improves the photocatalytic activity. Thus, we can consider that the optimum coating thickness is 400–500 nm, as larger thicknesses require a longer process and the improvement in photocatalytic activity is small, this optimal thickness is in agreement with that reported in other works [48].

3.1.6. Activity in successive photocatalytic cycles

The photocatalytic activity in the oxidation of NO(g) of the best performing coated-glass, **G3.3**, has been studied in successive photocatalytic cycles (Fig. 6). This coated-glass did not show stable photocatalytic behavior as a slight loss of photocatalytic activity was observed in consecutive cycles. Although the loss of activity is significant in the second photocatalytic cycle (**G3.3_rep2**), with a stabilization of the NO (g) concentration of 0.81 ppm, the loss of activity in the third cycle (**G3.3_rep3**) is very small, with a stabilization value for the NO(g) concentration of 0.85 ppm along the four hours of experiment. However, the initial decrease in NO(g) concentration gradually reduces in the successive photocatalytic cycles, which could be attributed to a decrease in porosity.

3.2. Characterization of porous TiO$_2$ photocatalytic coatings

The porous TiO$_2$ thin films deposited on glass have been analyzed by X-ray diffraction (XRD), Raman scattering, UV–vis spectroscopy,
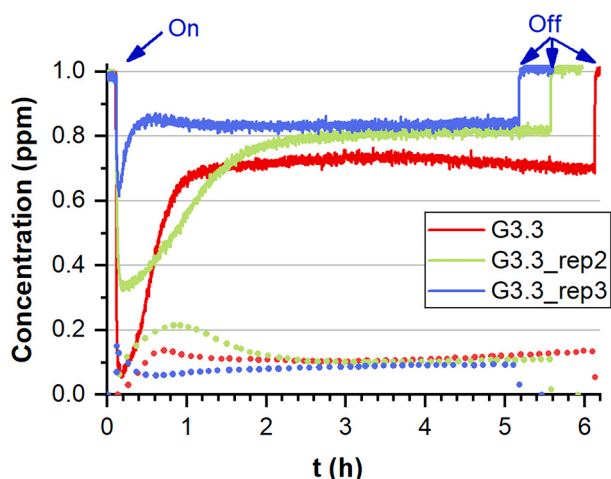
Fig. 6. Activity of coated-glass **G3.3** in three successive photocatalytic cycles. Degradation of NO(g) (solid line) and formation of NO$_2$(g) (dotted line).

Scanning Electron Microscopy (SEM) and High-Resolution Transmission Electron Microscopy (HRTEM) techniques.

The XRD diffractogram of "as deposited" coated-glass **G3** showed no crystalline diffraction peaks. The structure of the TiO$_2$ thin film is changed from amorphous to crystalline anatase after annealing at 550 °C following the temperature program described in the Experimental section [49,50]. The XRD pattern of **G3** (Fig. 7) showed the characteristic peaks of TiO$_2$ anatase at 2θ: 25.2, 36.8, 37.7, 38.5, 48.0, 53.8 and 55.0° [51]. The presence of the TiO$_2$ anatase phase in the coatings was further confirmed by the Raman spectra which showed four strong characteristic bands at 138, 390, 511 and 635 cm^{-1} [52]. The overlay of the Raman spectra of coated-glasses **G1-G4** is shown in Fig. 8. The amount of anatase in glass **G3** is higher than in glasses **G1** and **G2**, which is consistent with its higher photocatalytic activity. However, coated-glass **G4**, which contains a significant amount of anatase, showed a photocatalytic activity similar to **G2**, which is attributed to the presence of the rutile TiO$_2$ phase, as shown by the bands at 433 and 610 cm^{-1}, and a higher presence of metallic Ti due to sub-oxidation of the film.

The overlay of the Raman spectra of coated-glasses fabricated under different argon flows, deposition power and oxygen flows are shown in Figs. S3-S5 in the Supplementary Material. The amount of anatase in glasses **G3.2** and **G3.3** is higher than in glass **G3.4**, which is consistent with their higher photocatalytic activity. On the other hand, the amount of anatase in glass **G3.2c** is much higher than in glasses **G3.2a** and
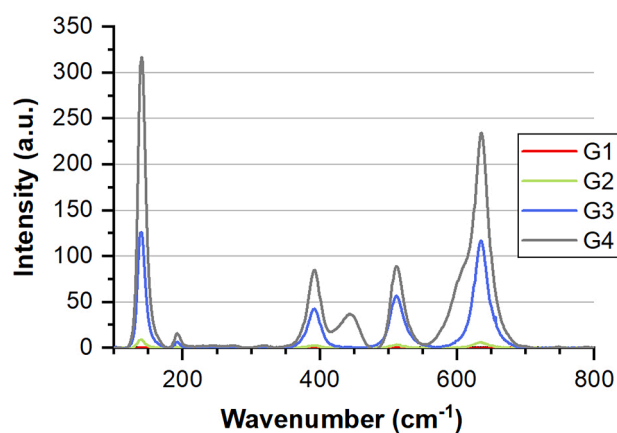

Fig. 8. Overlay of the Raman spectra of coated-glassed **G1-G4**.

G3.2b. The good photocatalytic performance of coated-glasses **G3.4** and **G3.2b** contrasts with their relatively low anatase content, which is attributed to the higher porosity of the coatings. Oxygen flow influence in Raman spectra is consistent with the photocatalytic activity shown in Fig. 5.

The UV–Vis. absorption spectrum of coated-glass **G3** with the highest photocatalytic activity is shown in Fig. 9. The spectrum shows a strong absorption region (<350 nm) and a strong transmittance region (>380 nm). The calculated optical band gap according to the Tauc method was 3.38 eV [12b]. The calculated band gaps of coated-glasses **G2** and **G4** were 3.65 and 2.81 eV, respectively. The smaller band gap of **G4** compared to **G3** is attributed to a significant amount of rutile TiO$_2$ phase in the coating (see above) [53] and coating sub-oxidation that increases the presence of metallic Ti. On the other hand, the band gap range in the series **G3.1** – **G3.4** and **G3.2a** – **G3.2c** was 3.38–3.63 eV (see Table S1 and Figs. S6-S12 in the Supplementary Material), the glass with the highest photocatalytic activity being the one with the smallest bandgap.

To determine the composition and identify the chemical states of the porous TiO$_2$-anatase photocatalytic coatings, quantitative XPS analysis was performed on coated-glasses **G3.2** and **G3.4**. The XPS general spectra of both samples showed, in addition to the Ti 2p and O 1s peaks, the C 1s peak due to adventitious carbon (Fig. S13 in the Supplementary Material). The Ti 2p and O 1s regions of the high resolution XPS spectra of the coated-glass **G3** (note that **G3.2** is the same sample as **G3**) are shown in Fig. 10.

The Ti 2p$_{1/2}$ and Ti 2p$_{3/2}$ spin-orbital splitting photoelectrons are located at binding energies of 464.3 and 458.6 eV, respectively. The peak positions and the peak separation of 5.7 eV of the Ti 2p doublet
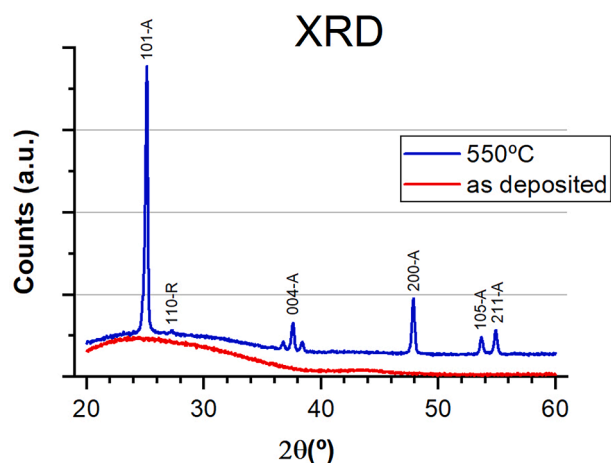

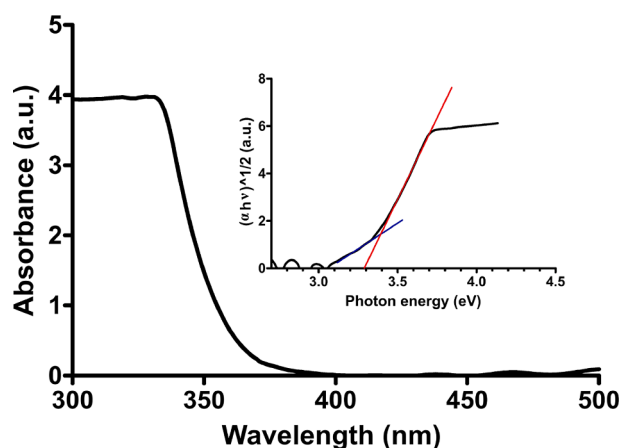**Fig. 7.** XRD pattern of coated-glass **G3**: as deposited (red line) and after thermal annealing at 550 °C (blue line).

Fig. 9. UV–vis. absorption spectra of coated-glass **G3**. Insets show band gap determination using the Tauc plot.
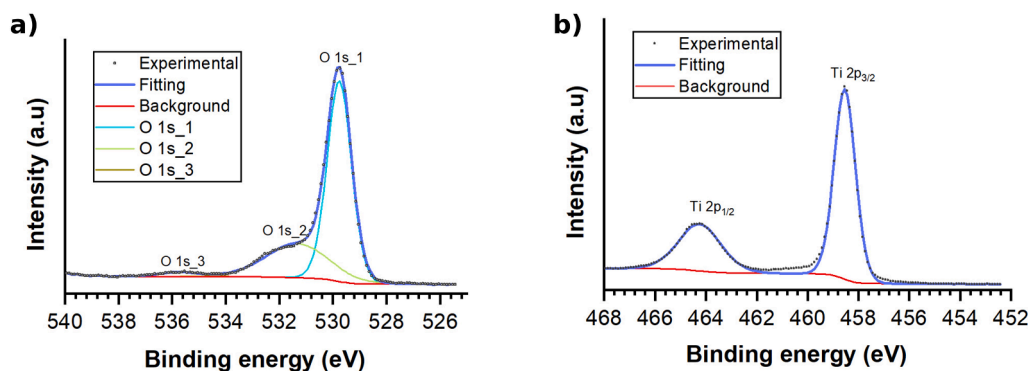
Fig. 10. High-resolution XPS spectra of the Ti 2p and O 1s peaks of the coated-glass **G3**. a) O 1s peak, b) Ti 2p peak.

agree well with the energy reported for TiO_2 particles [54,55]. Interestingly, reduced titanium species have not been detected in the Ti 2p spectrum. The O 1s signal shows a main peak at 529.8 eV and a shoulder located toward the side of higher binding energies. Peak deconvolution of the signal showed three peaks at binding energies of 529.8, 531.3 and 535.8 eV. The first peak at 529.8 eV corresponds to lattice bulk oxide (O^{2-}) whereas the remaining peaks result from the presence of water molecules on the sample surface. In particular, the peak with binding energy of 531.3 eV is assigned to the presence of hydroxyl (OH) groups on the surface whereas that at 535.8 eV correspond to water molecules on the surface [56]. The ratio of titanium to oxygen in **G3** was determined by integrating the areas under the Ti 2p and the main O 1s peaks. The titanium-to-oxygen ratio was 0.55:1, which is close to that expected from the stoichiometry of TiO_2. High resolution XPS spectra of the coated-glasses show similar characteristics confirming the presence of TiO_2 on the surface and the absence of reduced titanium species.

A top-view of the coated-glass **G3** at a magnification of 40.000 is shown in Fig. 11. The film is composed by grains of approximately 70–100 nm in diameter separated by empty zones of about 10–20 nm (dark areas). This surface microstructure with empty space between adjacent granules provides porosity to the film and is responsible for the observed photocatalytic activity. Coated-glasses showing good photocatalytic performance also exhibit a mosaic-like surface microstructure (see Figs. S14-S19 in the Supplementary Material).

Fig. 12 shows the cross section of sample **G3** visualized under the STEM microscope. The image confirms a film thickness of approximately 600 nm, which is consistent with the measurement obtained by mechanical profilometry. The morphology of the film is clearly columnar with fissures that confirm the porosity of the coating. The columnar structures have an inclination of approximately 77° produced by the oblique angle deposition. Magnification of the cross-sectional TEM
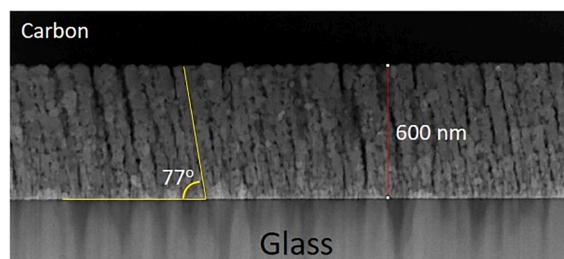

Fig. 12. Cross-section STEM imagen of coated-glass **G3**.

image showed the presence of small pores of 5–20 nm in diameter in addition to the columnar structures. Furthermore, TEM and HRTEM showed the polycrystalline nature of the film and the electron diffraction pattern confirmed that the coating composition is TiO_2 and corresponds to the anatase phase (see Figs. S20-S23 in the Supplementary Material).

4. Conclusions

Deposition of porous TiO_2-coatings on soda-lime glasses was achieved by sputtering physical vacuum deposition. It has been proven that, in order to have photocatalytic activity in the oxidation of NO, it is necessary to obtain TiO_2 in the anatase phase, for which a thermal treatment at a temperature of approximately 550 °C is essential. The effect of different deposition conditions on the photocatalytic activity has been studied. Among them, the use of an oblique angle deposition is essential to obtain porous films, which is of paramount importance to achieve photocatalytic activity. It has been shown that the ideal deposition angle is 60-65°, since there is a compromise between the porosity thus obtained, the thickness of the coating and the level of oxidation. Total pressure of the deposition process has been shown to be relevant, because the films deposited with a higher partial pressure have shown greater photocatalytic activity due to the deposition of less dense coatings of greater porosity. Finally, the oxygen flow during the deposition process must be carefully adjusted for each deposition conditions, since modification of any deposition parameter modifies the optimum oxygen flow.

The coated-glasses have been applied for the in-flow photocatalytic oxidation of nitrogen oxide. Maximum photocatalytic activity was achieved with a minimum porous film thickness of approximately 250 nm. The best performing coated-glass was able to reduce the NO concentration ca. 20 % for 5 h, although a slight loss of photocatalytic activity was observed in consecutive cycles. SEM and TEM images showed a surface microstructure composed of nanometric grains and a tilted columnar structure. Nanocrystal electron diffraction, XRD and Raman spectroscopy confirm the deposition of TiO_2 anatase, which, together with the porosity of the material, account for the observed photocatalytic activity.
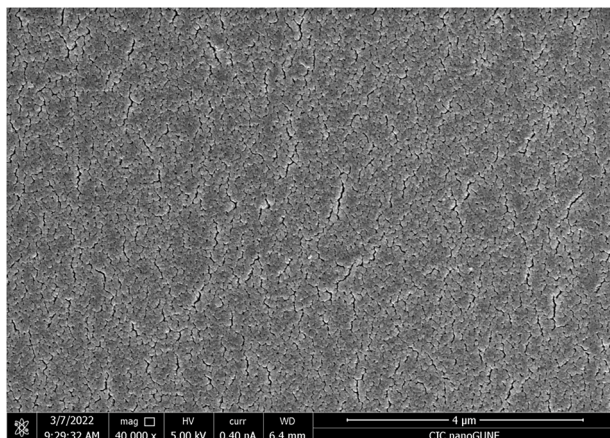

Fig. 11. Top-view FESEM imagen of coated-glass **G3**.

An interesting future step would be to find deposition conditions to obtain a photocatalytic coating deposited by dynamic sputtering that would allow the large-scale industrialization of the deposition process.

CRediT authorship contribution statement

Ramón Azpiroz: Methodology, Investigation. **Enrique Carretero:** Conceptualization, Methodology, Writing – original draft, Writing – review & editing. **Ana Cueva:** Methodology, Investigation. **Aida González:** Funding acquisition. **Manuel Iglesias:** Conceptualization, Writing – original draft, Writing – review & editing, Funding acquisition. **Jesús J. Pérez-Torrente:** Conceptualization, Methodology, Writing – original draft, Writing – review & editing, Funding acquisition.

Declaration of Competing Interest

The authors declare the following financial interests/personal relationships which may be considered as potential competing interests: J. J. Perez-Torrente reports financial support was provided by Spain Ministry of Science and Innovation. Enrique Carretero reports financial support was provided by Government of Aragon. J.J. Perez-Torrente reports financial support was provided by Government of Aragon.

Data availability

Data will be made available on request.

Acknowledgements

Appendix A. Supplementary data

Supplementary data to this article can be found online at https://doi.org/10.1016/j.apsusc.2022.154968.

References

[1] I. Manisalidis, E. Stavropoulou, A. Stavropoulos, E. Bezirtzoglou, Environmental and health impacts of air pollution: a review, Front. Public Health 8 (2020) 14, https://doi.org/10.3389/fpubh.2020.00014.

[2] P. Brimblecombe. The Effects of Air Pollution on the Built Environment, Imperial College Press, Imperial College Press, Cambridge, 2003.

[3] J.H. Seinfeld, S.N. Pandis. Atmospheric Chemistry and Physics: From Air Pollution to Climate Change, Wiley, New York, 1998.

[4] R.M. Harrison, R.E. Hester. Air Quality in Urban Environments, Royal Society of Chemistry, Cambridge, 2009.

[5] S. Wang, et al., Preferentially oriented Ag-TiO_2 nanotube array film: An efficient visible-light-driven photocatalyst, J. Hazard. Mater. 399 (123016) (2020), https://doi.org/10.1016/j.jhazmat.2020.123016.

[6] J. Fermoso, B. Sánchez, S. Suarez, Air purification applications using photocatalysis. Nanostructured Photocatalysts: From Materials to Applications in Solar Fuels and Environmental Remediation, Elsevier, 2020, pp. 99–128.

[7] Y. Wang, et al., Review of the progress in preparing nano TiO2: An important environmental engineering material, J. Environ. Sci. 26 (2014), https://doi.org/10.1016/j.jes.2014.09.023.

[8] J. Lasek, et al., Removal of NOx by photocatalytic processes, J. Photochem. Photobiol. C: Photochem. 14 (2013) 29–52, https://doi.org/10.1016/j.jphotochemrev.2012.08.002.

[9] C. Chen, P. Li, G. Wang, Y. Yu, F. Duan, C. Chen, We. Song, Y. Qin, M. Knez, Nanoporous Nitrogen-Doped Titanium Dioxide with Excellent Photocatalytic Activity under Visible Light Irradiation Produced by Molecular Layer Deposition, Angew. Chem. Int. Ed. 52 (2013) 9196–9200, https://doi.org/10.1002/ange.201302329.

[10] D.A.H. Hanaor, C.C. Sorrell, Review of the anatase to rutile phase transformation, J. Mater. Sci. 46 (2011) 855–874, https://doi.org/10.1007/s10853-010-5113-0.

[11] ISO 22197-1: 2007, Fine ceramics, advanced technical ceramics – test method for air-purification performance of semiconducting photocatalytic materials. Part 1: Removal of Nitric Oxide, International Organization for Standardization: Geneva, Switzerland, 2007. Note that ISO 22197-1: 2007 has been updated by ISO 22197-1: 2016.

[12] O. Carp, C.L. Huisman, A. Reller, Photoinduced reactivity of titanium dioxide, Prog. Solid State Chem. 32 (2004) 33–177, https://doi.org/10.1016/j.progsolidstchem.2004.08.001.

[13] M. Chen, J.-W. Chu, NOx photocatalytic degradation on active concrete road surface – from experiment to real-scale application, J. Cleaner Product. 19 (2011) 1266–1272, https://doi.org/10.1016/j.jclepro.2011.03.001.

[14] Y. Hu, et al., Local Structures of Active Sites on Ti-MCM-41 and Their Photocatalytic Reactivity for the Decomposition of NO, Catal. Lett. 90 (2003) 161–163, https://doi.org/10.1023/B:CATL.0000004111.02392.75.

[15] P.J. Kelly, R.D. Arnell, Magnetron sputtering: a review of recent developments and applications, Vacuum 56 (2000) 159–172, https://doi.org/10.1016/S0042-207X (99)00189-X.

[16] A. Demeter, et al., Visible-light photocatalytic activity of TiO_xN_y thin films obtained by reactive multi-pulse High Power Impulse Magnetron Sputtering, Surf. Coat. Technol. 324 (2017) 614–619, https://doi.org/10.1016/j.surfcoat.2016.10.011.

[17] W.J. Zhang, et al., Properties of TiO2 thin films prepared by magnetron sputtering, J. Mater. Sci. Technol. 18 (2002).

[18] D. Rafieian, et al., Controlled formation of anatase and rutile TiO2 thin films by reactive magnetron sputtering, AIP Adv. (2015), https://doi.org/10.1063/1.4931925.

[19] D. Ponnusamy, et al., Porous Anatase TiO2 Thin Films for NH3 Vapour Sensing, J. Electron. Mater. 44 (2015), https://doi.org/10.1007/s11664-015-4099-4.

[20] P.P. Pansila, et al., Preparation of Pure Anatase TiO2 Thin Films by DC Sputtering Technique: Study on the Effect of Oxygen Partial Pressure, Adv. Mater. Res. (2012), https://doi.org/10.4028/www.scientific.net/AMR.463-464.1415.

[21] M.R. Ranade, et al., Energetics of nanocrystalline TiO2, Colloquium 99 (2002), https://doi.org/10.1073/pnas.251534898.

[22] H. Zhang, et al., The size dependence of the surface free energy of titania nanocrystals, Phys. Chem. Chem. Phys. 11 (2009), https://doi.org/10.1039/B819623K.

[23] H. Zhang, et al., Understanding Polymorphic Phase Transformation Behaviour during Growth of Nanocrystalline Aggregates: Insights from TiO2, J. Phys. Chem. B 104 (2000), https://doi.org/10.1021/jp000499j.

[24] X.-Z. Ding, et al., Correlation Between Anatase-to-rutile Transformation and Grain Growth in Nanocrystalline Titania Powders, J. Mater. Res. 13 (1998), https://doi.org/10.1557/JMR.1998.0356.

[25] S.L. Isley, R.L. Penn, Penn, Relative Brookite and Anatase Content in Sol-Gel Synthesized Titanium Dioxide Nanoparticles, J. Phys. Chem. B 110 (2006), https://doi.org/10.1021/jp061417f.

[26] D. Pjević, et al., Properties of sputtered TiO2 thin films as a function of deposition and annealing parameters, Physica B 463 (2015), https://doi.org/10.1016/j.physb.2015.01.037.

[27] E.P. Ferreira-Neto, et al., Thermally stable SiO2@TiO2 Core@shell nanoparticles for application in photocatalytic self-cleaning ceramic tiles, Mater. Adv. 2 (2021), https://doi.org/10.1039/D0MA00785D.

[28] Y. Ma, et al., Titanium Dioxide-Based Nanomaterials for Photocatalytic Fuel Generations, Chem. Rev. 114 (2014), https://doi.org/10.1021/cr500008u.

[29] Y. Wang, B. Li, C. Zhang, L. Cui, S. Kang, X. Li, L. Zhou, Ordered mesoporous CeO2-TiO2 composites: Highly efficient photocatalysts for the reduction of CO2 with H2O under simulated solar irradiation, Appl. Catal. B Environ. 130–131 (2013) 277–284, https://doi.org/10.1016/j.apcatb.2012.11.019.

[30] D. Ren, et al., Study in the porosity of the TiO2 films prepared by magnetron sputtering deposition. 3rd International Nanoelectronics Conference (INEC), IEEE, 2010.

[31] R. Alvarez, et al., On the Deposition Rates of Magnetron Sputtered Thin Films at Oblique Angles, Plasma Process. Polym. 11 (2014), https://doi.org/10.1002/ppap.201300201.

[32] M. Horakova, et al., Sputter Deposition of Nanostructured TiO2 Thin Films, IEEE Trans. Plasma Sci. 42 (2014), https://doi.org/10.1109/TPS.2014.2326896.

[33] A. Barranco, et al., Perspectives on oblique angle deposition of thin films: From fundamentals to devices, Prog. Mater. Sci. 76 (2016), https://doi.org/10.1016/j.pmatsci.2015.06.003.

[34] J. Thornton, Influence of Apparatus Geometry and Deposition Conditions on Structure and Topography of Thick Sputtered Coatings, J. Vac. Sci. Tech. 11 (1974), https://doi.org/10.1116/1.1312732.

[35] J. Thornton, The Microstructure of Sputter-Deposited Coatings, J. Vac. Sci. Technol. A 4 (1986), https://doi.org/10.1116/1.573628.

[36] C.G. Kuo, et al., Photocatalytic characteristics of TiO2 films deposited by magnetron sputtering on polycarbonate at room temperature, Appl. Surf. Sci. 258 (2012), https://doi.org/10.1016/j.apsusc.2012.03.142.

[37] D. Rafieian, et al., Intrinsic Photocatalytic Assessment of Reactively Sputtered TiO2 Films, ACS Appl. Mater. Interfaces 7 (2015), https://doi.org/10.1021/acsami.5b01047.

[38] L.C. Escaliante, et al., Stability of the Photocatalytic Activity of TiO2 Deposited by Reactive Sputtering, Materials Research. 24 (2021), https://doi.org/10.1590/1980-5373-MR-2021-0051.

[39] D. Dumitriu, A.R. Bally, C. Ballif, P. Hones, P.E. Schmid, R. Sanjinés, F. Lévy, V. I. Pârvulescu, Photocatalytic degradation of phenol by TiO$_2$ thin films prepared by sputtering, (25) 2000 83–92. https://doi.org/10.1016/S0926-3373(99)00123-X.

[40] S. Biswas, K. Prabakar, T. Takahashi, T. Nakashima, Y. Kubota, A. Fujishima, Study of photocatalytic activity of TiO$_2$ thin films prepared in various Ar/O$_2$ ratio and sputtering gas pressure, J. Vac. Sci. Technol. 25 (2007) 912–916, https://doi.org/10.1116/1.2717194.

[41] B.R. Weinberger, R.B. Garber, Titanium dioxide photocatalysts produced by reactive magnetron sputtering, Appl. Phys. Lett. 66 (1995) 2409–2411, https://doi.org/10.1063/1.113956.

[42] H.S. Russell, L.B. Frederickson, O. Hertel, T. Ellermann, S.S.A. Jensen, Review of photocatalytic materials for urban NO$_x$ remediation, Catalysts 11 (2021) 675, https://doi.org/10.3390/catal11060675.

[43] R. Azpiroz, M. Borraz, A. González, C. Mansilla, M. Iglesias, J.J. Pérez-Torrente, Photocatalytic activity in the in-flow degradation of NO on porous TiO$_2$–coated glasses from hybrid inorganic-organic thin films prepared by a combined ALD/MLD deposition strategy, Coatings 12 (2022) 488, https://doi.org/10.3390/coatings12040488.

[44] M. Schaffer, B. Schaffer, Q. Ramasse, Sample preparation of atomic-resolution STEM at low voltages by FIB, Ultramicroscopy 114 (2012) 62–71, https://doi.org/10.1016/j.ultramic.2012.01.005.

[45] P. Makuła, M. Pacia, W. Macyk, How to correctly determine the band gap energy of modified semiconductor photocatalysts based on UV–Vis spectra, J. Phys. Chem. Lett. 9 (2018) 6814–6817, https://doi.org/10.1021/acs.jpclett.8b02892.

[46] M. Buchalska, M. Surówka, J. Hämäläinen, T. Iivonen, M. Leskelä, W. Macyk, Photocatalytic activity of TiO$_2$ films on Si support prepared by atomic layer deposition, Catal. Today 252 (2015) 14–19, https://doi.org/10.1016/j.cattod.2014.09.032.

[47] F. Guanghui, D. Jiafeng, P. Donghui, H. Ouli, The migration of alkali ions from glass substrates coated with sol-gel barrier films, J. Non-Cryst. Solids 112 (1989) 454–457, https://doi.org/10.1016/0022-3093(89)90572-3.

[48] M. Pérez-González, M. Morales-Luna, J. Santoyo-Salazara, H. Crotte-Ledesma, P. E. García-Tinoco, S.A. Tomás, Improved adsorption and photocatalytic removal of methylene blue by MoO$_3$ thin films: Role of the sputtering power, film thickness, and sputtering working pressure, Catal. Today 360 (2021) 138–146, https://doi.org/10.1016/j.cattod.2019.06.003.

[49] S. Gurakar, et al., Variation of structural and optical properties of TiO$_2$ films prepared by DC magnetron sputtering method with annealing temperature, J. Mater. Sci. Eng. B. 262 (2020), https://doi.org/10.1016/j.mseb.2020.114782.

[50] R.M. Nagabharana, et al., Effect of thermal annealing on structural and electrical properties of TiO2 thin films, Thin Solid Films 710 (2020), https://doi.org/10.1016/j.tsf.2020.138262.

[51] JCPDS-International Centre for Diffraction Data-2000 database.

[52] F.D. Hardcastle, Raman Spectroscopy of Titania (TiO$_2$) Nanotubular Water-Splitting Catalysts, J. Ark. Acad. Sci. 65 (2011), https://doi.org/10.54119/jaas.2011.6504.

[53] T. Luttrell, S. Halpegamage, J. Tao, A. Cramer, E. Sutter, M. Batzill, Why is anatase a better photocatalyst than rutile? - Model studies on epitaxial TiO$_2$ films, Sci. Rep. 4 (2014) 4043, https://doi.org/10.1038/srep04043.

[54] P. Krishnan, et al., Characterization of photocatalytic TiO$_2$ powder under varied environments using near ambient pressure X-ray photoelectron spectroscopy, Sci. Rep. 7 (2017), https://doi.org/10.1038/srep43298.

[55] B. Erdem, et al., XPS and FTIR Surface Characterization of TiO2 Particles Used in Polymer Encapsulation, Langmuir 17 (2001), https://doi.org/10.1021/la0015213.

[56] P. Krishnan, M. Liu, P.A. Itty, L. Zi, V. Rheinheimer, M.-H. Zhang, P.J.M. Monteiro, L.E. Yu, Characterization of photocatalytic TiO$_2$ powder under varied environments using near ambient pressure X-ray photoelectron spectroscopy, Sci. Rep. 7 (2017) 43298, https://doi.org/10.1038/srep43298.